Structural and Geochemical Characteristics of Faulted Sediments and Inferences on the Role of Water in Deformation, Rio Grande Rift, New Mexico

Data Repository Item

Supplementary Information on Fault Displacement, Age, Slip Rate, Shape, Orientation, Kinematics, Fault Component Width Distributions and Relationships to Displacement, and Permeametry

Jonathan Saul Caine and Scott A. Minor, U.S. Geological Survey, Denver, Colorado, 80225

Introduction

The following data repository material supplements the paper *Structural and Geochemical Characteristics of Faulted Sediments and Inferences on the Role of Water in Deformation, Rio Grande Rift, New Mexico.* It covers details on a variety of methods, data, calculations, and plots that address additional geologic characteristics of the fault zone and the stratigraphic package it cuts, the age of faulting, pertinent details on the relationships between fault zone component widths and dip separation, frequency distribution of fault zone component widths, and permeametry results not presented in the main paper. All of the raw data used in the main paper are also included here.

Additional Geologic Characteristics of the San Ysidro Fault

Growth Faulting and Age

Connell et al. (1999) discussed the possibility that some units thicken eastward of the San Ysidro fault and thus suggested that faulting was syndepositional. This would imply that the San Ysidro is a growth fault that ruptured the ground surface at the time these units were deposited. However, we did not find compelling evidence for growth faulting along the San Ysidro. A

growth fault hypothesis can only be tested by comparing the stratigraphic thickness of the Cerro Conejo Member of the Zia Formation (Tzcc, Figures DR1 and DR2) on either side of the fault because it is the only unit that is present in both the hanging-wall and footwall blocks. Younger units are eroded from the footwall block and the basal portions of the older units are not exposed in the hanging-wall block, limiting cross-fault thickness comparisons. Based on the geologic mapping of Connell et al. (1999), estimates of Tzcc thicknesses are 227 m on the footwall side adjacent to the fault, 254 m on the hanging-wall side adjacent to the fault, and 309 m a few kilometers east of the fault with estimate error of about +/- 20 m. Although these few estimates do suggest an eastward thickening of Tzcc, the thickening appears to be gradual rather than abrupt across the fault. This comparison of thickness across the fault, the amount of error associated with the estimates, and the fault rock textures discussed below indicate that it is ambiguous if the San Ysidro was a surface-rupturing growth fault.

Constraining the temporal evolution of the fault also is difficult. The maximum dip-slip displacement on the fault is approximately 680 m and we assume that it occurred episodically and syntectonically with the growth of the Rio Grande rift. If the fault started growing during deposition of the oldest rift-related sediment, the Cerro Conejo Formation (Tzcc), the maximum age of the fault would be ~11 Ma based on dated ash beds within Tzcc that are cut by the fault (Connell et al., 1999). This yields an average, minimum displacement rate of ~0.06 mm/yr. However, there are no real constraints on whether or not the fault was active during Cerro Conejo time and thus the fault could be younger. If we assume that faulting initiated when the youngest of the rift-filling sediments, the upper Miocene Picuda Peak Member of the Arroyo Ojito Formation were deposited, the fault would have a maximum age of ~6.5 Ma (Connell, 2006) and an average, minimum displacement rate of ~0.1 mm/yr. On the Llano de Albuquerque

plateau, just south of the fault exposures investigated in this study, deposits of the Plio-Pleistocene Ceja Formation are displaced ~75 m by the San Ysidro fault (Connell, 2006), indicating that about 11% of the total fault displacement occurred after about 1.8 Ma with a minimum displacement rate of ~0.04 mm/yr. These end member slip rates are consistent with those reported for the fault by Kelson and Personius (1997). Holocene sand deposits (Qs, Figure DR1) are not cut by the fault and thus provide a minimum age of fault movement.

Fault Trace Characteristics, Orientation Data, and Fault Kinematics

At a map scale of 1:24,000, the San Ysidro fault is largely planar with a few curviplanar sections (Figure DR1). Simple estimates of the shape of the fault trace can be derived from measurements of amplitude-wavelength ratios for the curviplanar sections of the trace. These ratios show a bimodal frequency distribution with maxima (modes) at 0.07 and 0.17 for n=19. The lower mode may reflect local protolith heterogeneities such as small curvatures in the fault trace caused by the juxtaposition of lithologies with contrasting strengths. The higher mode and greater curvatures may represent linked segments boundaries (Figure DR1). One probable linked segment boundary is located near the northern end of the fault exposure in an area we call the "horsetail", which is most likely a left-stepping segment boundary and abandoned tip zone where the fault has curved to the west and linked with another north-trending segment (Figure DR1). A second possible linked segment boundary exists in the central part of the fault exposure where it takes a large jog to the west near several small, northeast-striking faults in the adjacent hanging wall block (Figure DR1).

Figure DR1 and Table DR1 show detailed orientation data for fault-zone structures (bedding, core-bounding and intra-core slip surfaces, distributed slip surfaces in the entrained and damage

zones, deformation bands, joints, veins, and clastic dikes) collected at individual localities aggregated for three contiguous segments of the San Ysidro fault: the horsetail, central, and southern segments. These sections of the fault zone are broken out to show along-strike variations in the orientation of the different structures. Bedding in the protolith well outside of the fault zone strikes north-northwest to west-southwest and dips shallowly to the west-southwest and south-southeast in all segments. The inclination of the beds in combination with large topographic relief creates a relatively large vertical exposure of the host sedimentary section. At a few footwall and hanging wall localities, bedding defines 'drag' folds at a variety of scales (Figures 2, 3, and 4). Within the fault zone, entrained bedding strikes subparallel to the fault with dips averaging 37º to the east (Figure DR1 and Table DR1). Quasi-conjugate Eigen vector mean orientations for small faults (slip surfaces with displacements generally less than one meter), deformation bands, and veins are consistent with those predicted by Anderson's Theory of Faulting (Anderson, 1905).

Slip lineation data from numerous localities along the fault indicate predominantly dip slip, down to the east-southeast relative displacement (Figure DR1 and Table DR1). Along strike, variation in the rake of slickenlines indicates variable subordinate components of strike slip that appear to be controlled by the geometry of the fault surface, particularly where it jogs left, such as at the horsetail. The horsetail is an area of broadly distributed deformation in the hanging wall. The structures in this area include closely spaced, short trace length, small-displacement faults that strike north to northeast with down to the east to southeast normal-dextral oblique slip (Figure DR1 and Table DR1). Slip lineations on the main fault surface bounding the west side of the horsetail zone abruptly change from dip slip to dextral-oblique slip at the point of maximum curvature of the left-stepping fault trace (Figure DR1 and Table DR1). Slip lineation data from

the small faults in the horsetail show a greater degree of dextral slip as compared to the main fault (Figure DR1 and Table DR1). These small faults emerge from the point of maximum curvature of the main San Ysidro fault trace where it begins to step westward, possibly at an abandoned segment boundary (Figure DR1). The horsetail faults, which die out to the north, are characterized by narrow zones of closely spaced deformation bands with intermittent clay-rich cores that are less than a few centimeters wide. The kinematics of the small faults, their point of emergence from the main fault, and their geometry relative to the main fault are consistent with an abandoned San Ysidro fault tip zone that has properties and kinematics similar to horsetail fractures at the outcrop to microscopic scales (e.g. Martel et al., 1988; Kim et al., 2004).

Details Regarding Fault Component Width-Displacement Relationships

Measurements of fault zone component widths were made in the field using a graduated tape placed at right angles to each component and adjusted using trigonometric calculations if necessary (Table DR2). Not all components were exposed in all traverses. In Table DR2, cells that are blank indicate a locality where the specified component width was not exposed. Cross sections were used to investigate if there is any systematic relationship between fault component width and dip separation, the latter a proxy for displacement (Grauch et al., 2006; Hudson et al., 2008; Figure 7 and Table DR3). Widths of the clay-rich fault core were measured at 35 locations along the strike of the fault and the total width of the fault including the footwall and hanging wall damage and entrained zones plus the core were measurable at seven locations (Table DR3). Because there are more core width measurements than dip separation estimates, we needed a method to estimate dip separation at locations with core width measurements that do not have corresponding separations measured directly from the cross sections. Thus, we chose to describe

variations in displacement along strike using a simple linear regression of dip separation versus position along strike (Figure 7). Although the cross-section-derived data suggest a non-linear displacement gradient along the strike of the fault, the linear regression computed from these data has a reasonable correlation factor (R^2) of 0.85, indicating its suitability for computing dip separation values. Table DR3 shows the resulting computed values of dip separation at those localities where the various fault core widths and total fault widths listed were measured; these data are plotted in Figure 7.

San Ysidro Fault and Protolith Permeability Structure

Methods

Representative samples of each component were collected along 7 traverses across the fault (Figure DR2) to investigate the permeability structure of the fault zone. Two methods were used to obtain permeability data from the sampled protolith and fault materials: core-plug liquid permeametry and, for fault core clay samples, mercury injection capillary entry pressure permeametry.

For the core-plug permeability measurements large, oriented block samples (typically about 30 cm on a side) of cemented and uncemented protolith, damage zone, and mixed zone sediments were collected to minimize biases that might result from smaller sample sizes. Surface weathering rinds were scraped off and the blocks of sediment were carved loose from the outcrops. The blocks were generally lithified enough to be bound by tape to insure preservation of the internal structure of the sample during transport. Cores were drilled from these blocks, both parallel and perpendicular to bedding, at TerraTek Inc., Salt Lake City, Utah, with core dimensions ranging from 3 to 4 cm in diameter and 6 to 8 cm in length.

Liquid permeability was determined using a hydrostatic load-confining vessel at TerraTek (ASTM D 5084, 2005). This method results in a direct measure of the absolute intrinsic permeability of the sample. Using pumped deionized water at a known temperature, the samples were flooded and a constant head gradient was maintained from the upstream to downstream ends of the sample. Differential pressures were measured once a steady state was achieved. Using the cross sectional area of the core sample at the downstream end, the head gradient, and Darcy's law, the hydraulic conductivity (property of both fluid and media) of the sample can be calculated. Using the temperature and pressure conditions of each test the fluid density and viscosity were determined and the intrinsic permeability (media property only) of the samples was derived from the hydraulic conductivity data (Figure DR3). Confining and pore pressures during the tests were set to a net applied stress of 300 psi (2.1 MPa) in order to seal the sample in its pressure jacket and simulate near-surface flow conditions.

Due to the small size of exposed fault clay cores, their generally high degree of friability, and expected low permeability, mercury injection capillary entry pressure was used to estimate the permeability of these materials. Because unoriented samples of clay core were used for these analyses, permeability anisotropy within the fault core could not be evaluated. The analyses, which were completed by PetroTech Associates in Houston, Texas, employed a method that is a hydrocarbon industry standard for low permeability materials (e.g., Swanson, 1981). Samples of clay core approximately one cubic centimeter in size were placed in a pressure cell and flooded with mercury while the pressure in the cell was monitored. A plot of entry pressure versus time was monitored during the flooding. The plots show distinct peaks and plateaus where peak pressures correspond to grain-scale pore throats being flooded allowing flow-through of the mercury, and reflect the minimum permeability of the sample. An empirical relationship was

developed by Swanson (1981) to calculate intrinsic, liquid permeability of the sample as a function of entry pressure. Thus peak pressures for each sample were chosen and the corresponding permeability was calculated.

Data and Results

Figure DR3 show a composite of plot and data of all permeametry results for each San Ysidro fault component. The measured permeabilities range from $6.8x10^{-12}$ m^2 to $3.0x10^{-20}$ m^2. Geometric mean permeabilities from the clay-rich fault core are approximately six and one half orders of magnitude lower than the geometric mean permeabilities of uncemented protolith sand from either the footwall or hanging wall and approximately two orders of magnitude lower than cemented protolith, damage or mixed zones (Figure DR3). Geometric mean permeabilities of cemented protolith, damage or mixed zones are approximately four orders of magnitude lower than the uncemented protolith in either the hanging wall or footwall. Samples of the damage and mixed zones were only recoverable from the footwall, were always cemented, and have essentially the same geometric mean permeability (Figure DR3 and Table DR7). The geometric means of both cemented and uncemented protolith samples show that the hanging wall samples have about an order of magnitude higher permeability than those of the footwall. This is consistent with the field observation that hanging wall protolith sediments are generally coarser grained than those in the footwall (Hudson et al., 2008).

Data Repository References Cited

Anderson, E. M., 1905, The dynamics of faulting: Transactions of the Edinburgh Geological Society, v. 8, pp. 387-402.

Anderson, E. M., 1905, The dynamics of faulting: Transactions of the Edinburgh Geological Society, v. 8, pp. 387-402.

ASTM D 5084, 2005, Standard test methods for measurement of hydraulic conductivity of saturated porous materials using a flexible wall permeameter: ASTM International.

Caine, J. S. and Forster, C. B., 1999, Fault zone architecture and fluid flow: Insights from field data and numerical modeling, *in* Haneberg, W.C., Mozley, P. S., Moore, J. C. and Goodwin, L. B., eds., Faults and sub-surface fluid flow in the shallow crust: American Geophysical Union Geophysical Monograph 113, pp. 101-127.

Cather, S.M., Connell, S.D., Heynekamp, M.R., and Goodwin, L.B., 1997, Geology of the Sky Village SE 7.5 minute Quadrangle, Sandoval County, New Mexico: Socorro, New Mexico, New Mexico Bureau of Mines and Mineral Resources, Open-File Report DGM 9, 1 Sheet.

Connell, S.D., Koning, D.J., and Cather, S.M., 1999, Revisions to the stratigraphic nomenclature of the Santa Fe Group, northwestern Albuquerque Basin, New Mexico; Albuquerque geology: Guidebook – New Mexico Geological Society, v. 50, pp. 337-353.

Connell, S.D., compiler, 2006, Preliminary geologic map of the Albuquerque-Rio Rancho metropolitan area and vicinity, Bernalillo and Sandoval Counties, New Mexico: New Mexico Bureau of Geology and Mineral Resources Open-File Report 496, scale 1:50,000.

Grauch, V.J.S., Hudson, M.R., Minor, S.A., and Caine, J.S., 2006, Sources of along-strike variation in magnetic anomalies related to intrasedimentary faults: A case study from the Rio Grande Rift, USA: Exploration Geophysics, v. 37, pp. 372-378.

Hudson, M.R., Grauch, V.J.S., and Minor, S.A., 2008, Rock magnetic characterization of faulted sediments with associated magnetic anomalies in the Albuquerque basin, Rio Grande rift, New Mexico: Geological Society of America Bulletin, v. 120, 18 pp., doi: 10.1130/B26213.1

Kelley, V.C., 1977, Geology of Albuquerque Basin, New Mexico: New Mexico Bureau of Mines and Mineral Resources Memoir 33, 60 pp.

Kelson, K.I., and Personius, S.F., compilers, 1997, Fault number 2029b, Jemez-San Ysidro fault, San Ysidro section, in Quaternary fault and fold database of the United States: U.S. Geological Survey website, http://earthquakes.usgs.gov/regional/qfaults

Kim, Y-S., Peacock, D.C., and Sanderson, D.J., 2004, Fault damage zones: Journal of Structural Geology, v. 26, pp. 503-517.

Koning, D.J., Pederson, J., Pazzaglia, F.J., and Cather, S.M., 1998, Geology of the Cerro Conejo (Sky Village NE) 7.5-min. quadrangle, Sandoval County, New Mexico, New Mexico Bureau of Mines and Mineral Resources, Open-File Geologic Map Open File-GM 45, scale 1:24,000.

Martel, S.J., Pollard, D.D., and Segall, P., 1988, Development of simple strike-slip fault zones, Mount Abbot Quadrangle, Sierra Nevada, California: Geological Society of America Bulletin, v. 100, pp. 1451-1465.

Steinsund, P.I., 1995, StereoNet Version 3.0, Orientation data analysis computer code: Geological Software.

Swanson, B.F., 1981, A simple correlation between permeabilities and mercury capillary pressures: Journal of Petroleum Technology, v. 33, pp. 2498-2504.

Sweeney, R.E., Grauch, V.J.S., and Phillips, J.D., 2002, Merged digital aeromagnetic data for the middle Rio Grande and southern Espanola basins, New Mexico: U. S. Geological Survey Open-File Report 02-0205, 15 pp.

Figures

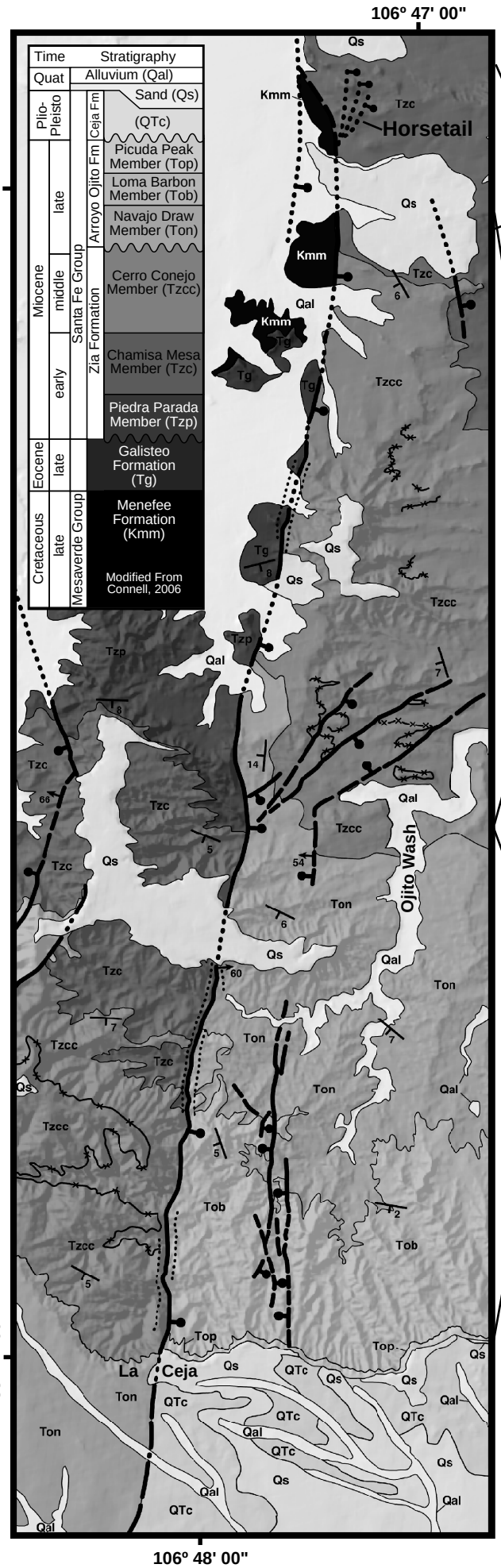

Horsetail Structures

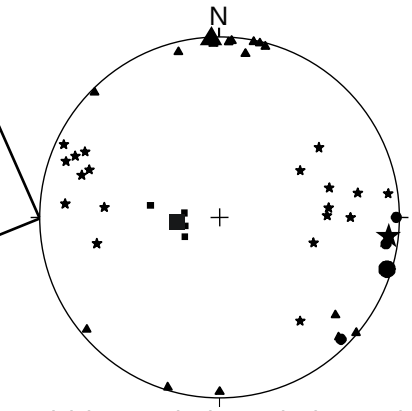

▪ Bd (4), ★DB (19), ▲ Jt (15), ● Vn (3)

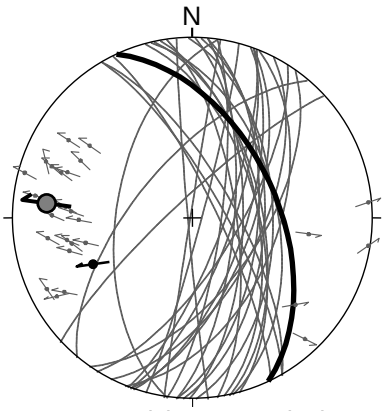

CSS (1), HSS (28)

Central Structures

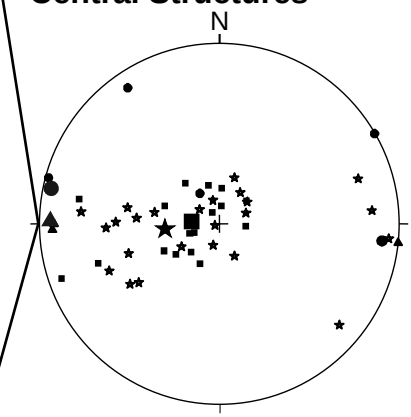

▪ Bd (18), ★ DB (24), ▲ Jt (3), ● Vn (5)

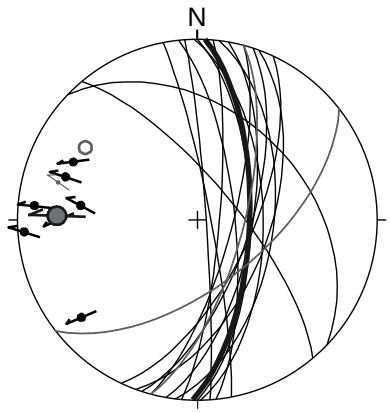

CSS (14), MZ/DZ SS (2)

Southern Structures

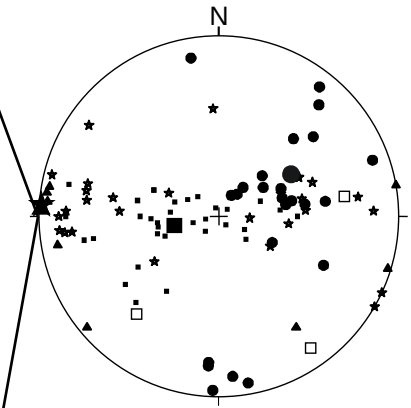

▪ Bd (32), ★ DB (28), ▲ Jt (8), ● Vn (24), □ CD (3)

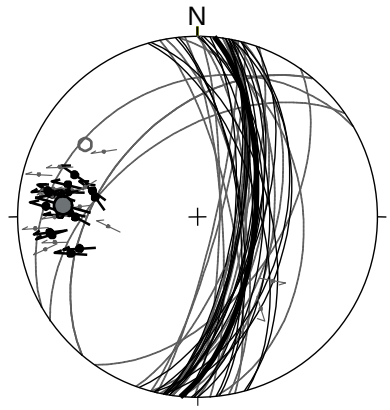

CSS (19), MZ/DZ SS (22)

EXPLANATION

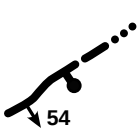

San Ysidro Fault: Solid where clay rich core is exposed,dashed where inferred from partial exposures and aeromagnetic data, dotted where concealed. Ball and bar on down dropped side. Arrow shows dip and dip direction.

Damage Zone Boundary (inclusive of mixed zone): Where partially exposed and inferred.

Sedimentary Contact

Strike, dip, and dip angle of beds.

Ash beds geochemically correlated with 11ma ashes from Idaho.

Figure DR1. Geologic map of the San Ysidro fault showing the local stratigraphic section and orientations of structures plotted on lower-hemisphere equal-area projections for the horsetail, central, and southern segments of the fault to illustrate structural changes between each segment. The mapped geology and stratigraphy is modified from Koning et al. (1998) and Connell et al. (1999) (Quat = Quaternary, Pleisto = Pleistocene, Fm = Formation). The topographic base is from U.S. Geological Survey Digital Elevation Model data, Cerro Conejo, New Mexico, 7.5' quadrangle. The first column of equal-area plots shows individual poles to each structural element as well as the Eigen vector mean orientations as enlarged symbols for each data set (Bd = bedding, DB = deformation bands, Jt = joints, Vn = veins, CD = clastic dikes; numbers in parentheses are the number of data points for each fabric element). The second column of equal-area plots shows slip surfaces (as great circles) and associated slickenlines (as tangent lineation symbols) measured along each segment of the fault. Arrows accompanying each tangent lineation pole indicate the movement direction of the footwall. Black great circles and tangent lineation symbols are for slip surfaces within and bounding fault cores (CSS) and gray circles and symbols are for distributed mixed zone (MZ) and damage zone (DZ) slip surfaces (SS) and horsetail slip surfaces (HSS). The mean slip surfaces and slip vectors for the core slip data from each fault segment are shown with wide black great circles and enlarged filled slip-linear symbols. Poles to the mean MZ/DZ slip surfaces from each fault segment are shown with large gray open circles.

Geologic Map Showing Cross Section Lines

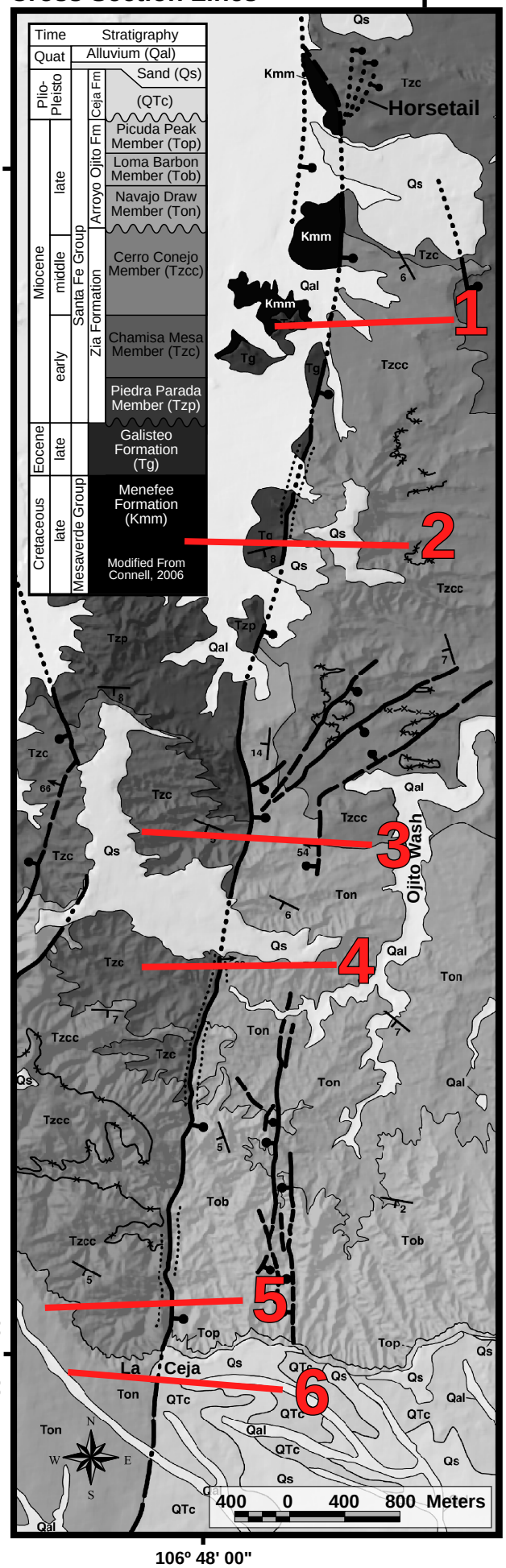

Cross Sections

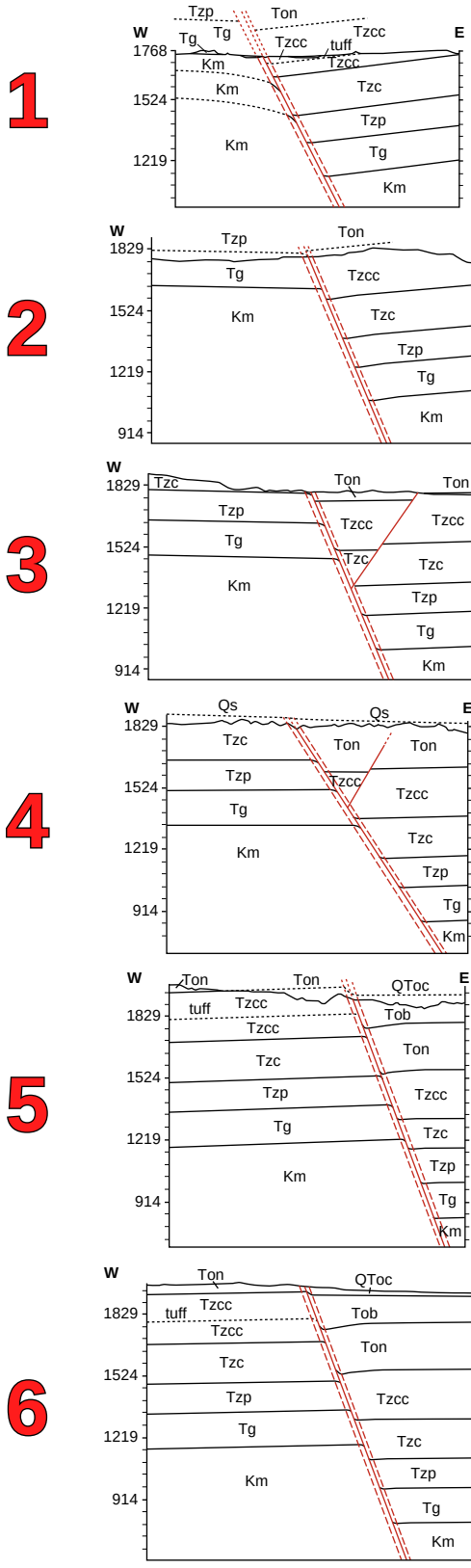

CROSS SECTION EXPLANATION (Map symbols on Figure DR1)

San Ysidro Fault Core: Solid clay core projected into subsurface, dotted where projected above ground surface.

Damage Zone Boundary: Dashed where projected into subsurface, dotted where projected above ground surface.

Sedimentary Contact or Tuffaceous Ash Bed: Ash dotted in subsurface, contacts dotted where projected above ground surface.

No Vertical Exaggeration (elevations in meters above mean sea level)

δ = Dip Separation Estimate

500 0 500 1000 meters

Figure DR2. Geologic cross sections constructed across the San Ysidro fault from which dip separations were estimated. Accompanying geologic map shows the location of the section lines.

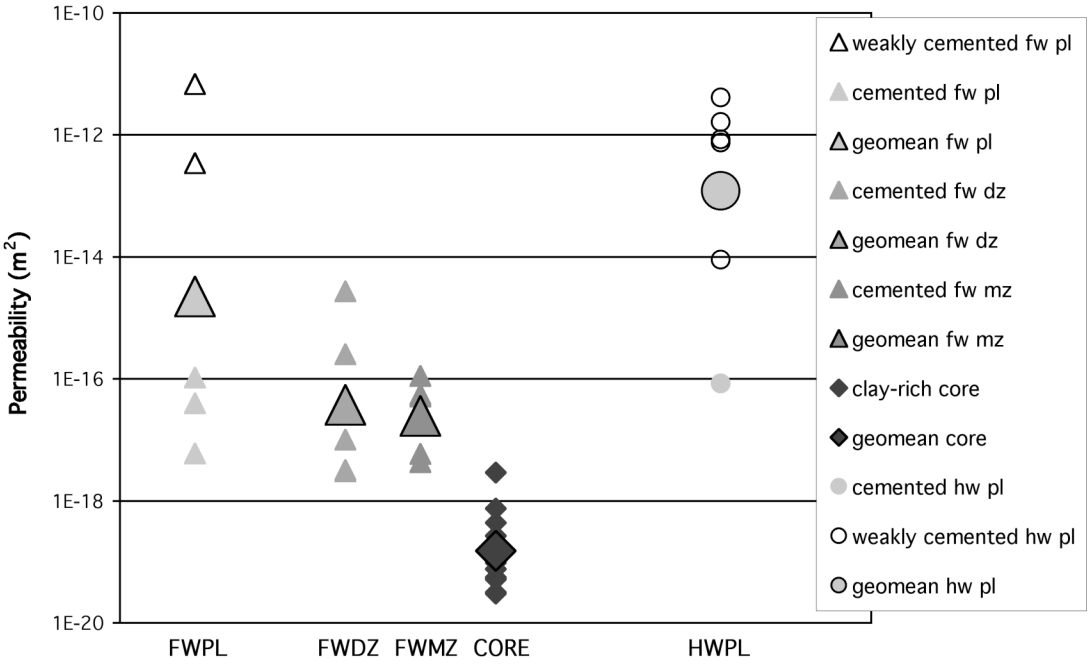

Figure DR3. Composite plot of all permeametry data for each component of the San Ysidro fault zone. Uncemented to weakly cemented samples are shown with small open symbols and cemented and clay-rich core samples are shown with small filled symbols. Geometric means of sample permeabilities for each fault component are shown with large filled symbols. Abbreviations: fw = footwall, hw = hanging wall, pl = protolith, dz = damage zone, mz = mixed zone, geomean = geometric mean.

Tables

Table DR1. San Ysidro Structural Orientation Data

Abbreviations: K = shape distribution indicating degree of clustering of data; high K values indicate a highly clustered distribution (Steinsund, 1995); n = number of data; all data reported using the right hand rule. For the full data set please contact the authors (jscaine@usgs.gov).

		Mean Eigen Vector		Mean Plane			
Location	**Structure**	**Plunge**	**Trend**	**Strike**	**Dip**	**K**	**n**
All	protolith bedding	86	266	356	5	31.4	23
All	damage and mixed zone bedding	53	261	350	37	7.5	26
All	fault core slip surfaces (mean rake = 97º)	25	272	2	66	7.03	39
All	mz / dz slip surfaces (mean rake = 72º)	20	278	8	70	2.34	53
All	deformation bands	14	274	4	76	0.19	72
All	joints	0	142	232	90	0.04	26
All	calcite veins	46	70	160	44	1.26	32
All	clastic dikes	25	116	206	65	0.09	3
Horsetail	bedding	70	266	356	20	2.09	4
Central	bedding	77	276	6	13	1.14	18
South	bedding	69	260	350	21	0.96	32
Horsetail	deformation bands	8	96	186	82	0.89	19
Central	deformation bands	65	266	356	25	0.52	24
South	deformation bands	1	274	4	89	0.25	28
Horsetail	distributed slip surfaces	20	276	6	70	3.87	28
Central	core slip surfaces	23	272	2	67	4.7	14
South	core slip surfaces	26	275	5	64	13.4	19
Horsetail	joints	0	357	87	90	0.44	15
Central	joints	6	271	1	84	1.36	3
South	joints	2	272	2	88	0.63	8
Horsetail	calcite veins	5	107	197	85	0.46	3
Central	calcite veins	5	282	12	85	1.21	5
South	calcite veins	52	52	142	38	0.5	24

Table DR2. Fault Component Width Data for the San Ysidro Fault in Meters

Abbreviations: m = meters, E = east, N = north, W = width, fw = footwall, dz = damage zone, mz = mixed zone, c = core, hw = hanging wall, t = total, min = minimum, n = number of samples, Blank Cells = data not measurable. Note: Locations in Universal Transverse Mercator North American Datum 1927.

mE	mN	Wfwdz	Wfwmz	Wc	Whwmz	Whwdz	Wc+Wmz fw	Wc+Wmz	Wt min
336648	3921599	26.3	7.5						
336680	3921823	0	3.5	2.3	0	3.2	5.8	5.8	9
336499	3921189	15.8	0.1	0.9	0	28.7	0.9	0.9	45.4
337191	3925169	11.3	1.3	0.1	0	13.1	1.4	1.4	25.8
337365	3925715	42	4.6	0.1	4.1	25.2	8.8	4.7	76
336321	3919311	3.9	0.2	3.5	0.2	2.4	3.9	3.7	10.2
336898	3923047			0.5					
336743	3922329			0.2	0	4			
336793	3922429	13.7	1.7	0.6	0	50.2	2.3	2.3	66.2
337591	3928351			1.4	0	17.1			
336377	3920125	59.8	1.8	0.03	0	37.9	1.9	1.9	99.6
337620	3927442			0.1					
337606	3927346			0.1					
336897	3924008			0.1					
336884	3923942			0.1					
336831	3923717			0.9					
336832	3923672			0.3					
336834	3923599		1	0.1				1.1	
336848	3923511			0.1					
336838	3923471			1.6					
336852	3923429			0.5					
336876	3923293		1	0.04				1	
336900	3923124			0.4					
336897	3923082			0.1					
336912	3923021			0.1					
336904	3922895		0.4	0.04				0.4	
336902	3922799		0.2						
336889	3922749		0.4	1				1.4	
336879	3922703			0.02					
336830	3922572		2	0.5				2.5	
336398	3920439		1.5	0.02				1.5	
336391	3920312		0	0.02				0	
336390	3920230		0	0.2				0.2	
336311	3919937			0.2					
336305	3919851			0.4					
336309	3919795			0.5					
336315	3919751			0.1					
	maximum	59.8	7.5	3.5	4.1	50.2	8.8	5.8	99.6
	minimum	0	0	0.02	0	2.4	0.9	0	9
	average	21.6	1.6	0.5	0.5	20.2	3.6	1.9	47.4
	median	14.8	1	0.2	0	17.1	2.3	1.4	45.4
	n	8	17	35	9	9	7	15	7

Table DR3. San Ysidro Fault Width - Displacement Relationships in Meters

Abbreviations: Loc = location, m = meters, E = east, N = north, EDS = estimated dip separation, n = number of data, W = width, c = core, CDS = computed dip separation, t = total, min = minimum. Note: Approximate estimated error associated with cross sections < 50 m and < 25 m associated with error of computed values. All locations in Universal Transverse Mercator, North American Datum 1927.

Dip Separation Data Estimated from Cross Sections and Position Along Fault Trace

Loc mE	Loc mN	EDS (m)
336215	3918620	440
336301	3919195	450
336689	3921776	600
336900	3922781	520
337532	3926703	680

Fault Width and Computed Dip Separation Using Regression: $y=0.03x-113463$, $R^2=0.85$

Clay-Rich Core Width, n = 35

Loc mN	Wc	CDS (m)
3921823	2.3	662
3921189	0.9	644
3925169	0.1	759
3925715	0.1	775
3919311	3.5	589
3923047	0.5	698
3922329	0.2	677
3922429	0.6	680
3928351	1.4	852
3920125	0.03	613
3927442	0.1	826
3927346	0.1	823
3924008	0.1	726
3923942	0.1	724
3923717	0.9	717
3923672	0.3	716
3923599	0.1	714
3923511	0.1	711
3923471	1.6	710
3923429	0.5	709
3923293	0	705
3923124	0.4	700
3923082	0.1	699
3923021	0.1	697
3922895	0	693
3922749	1	689
3922703	0	688
3922572	0.5	684
3920439	0	622
3920312	0	618
3920230	0.2	616
3919937	0.2	607
3919851	0.4	605
3919795	0.5	603
3919751	0.1	602

Total Fault Width, n = 7

Loc mN	Wt min	CDS (m)
3921823	9	662
3921189	45.4	644
3925169	25.8	759
3925715	76	775
3919311	10.2	589
3922429	66.2	680
3920125	99.6	613

TABLE DR4. X-Ray Diffraction Mineralogic Data for Components of the San Ysidro Fault Zone

ferruginous smectite, Ill = illite, Chlor = chlorite, Cal = calcite, Hem = hematite, fw = footwall, hw = hanging wall, pl = protolith, mz = mixed zone, dz = damage zone, dbs = deformation bands, mineralogy using the RockJock method = rj and sq = SIROQUANT method, see text for explanation.

Sample Number	Fault Zone Component	Lithology	Mineral (All Concentrations in Weight Percent)										XRD Method
			Qtz	K-Spar	Plag	Clay$_t$	Kao	Fe Smec	Ill	Chlor	Cal	Hem	
22202 5	clastic dike	uncemented calstic dike	71	11	12	6					0	0	sq
42901 C	clastic dike	weakly cemented clastic dike	35	15	13	2					36	0	sq
22002 9A	core	green clay	11	7	0	82	0	31	49	2	0	2	rj
22002 9C	core	tan clay	12	8	2	81	2	25	50	4	0	2	rj
40602 1	core	red clayey sand	50	6	6	19					15	1	sq
40602 10	core	red clay	18	2	3	71					0	0	sq
42601 B	core	red sandy clay	60	20	17	3					1	0	sq
90402 2B	core	tan sandy clay	44	23	18	15					1	0	sq
90402 2C	core	tan clay	24	11	1	54	1	11	39	3	0	2	rj
90602 7	core	red clay	35	8	1	53	5	18	28	2	2	3	rj
42901 D	fw mz	cemented sand	26	18	10	0					46	0	sq
42501 T1H	fw mz core contact	cemented sand	25	13	6	3					52	0	sq
22002 13A	fw pl	cemented sand	42	6	6	6					38	1	sq
40402 1	fw pl	cemented sand	43	3	14	0					39	0	sq
40602 8	fw pl	red clay	20	5	1	60	5	11	42	2	6	3	rj
40602 9	fw pl	weakly cemented sand	32	10	1	15					18	2	sq
42501 T1PL	fw pl	weakly cemented sand	51	17	19	10					0	0	sq
90402 1	fw pl	cemented sand	30	18	18	5					28	0	sq
22202 12	hw dz	weakly cemented sand	64	14	16	4					2	0	sq
40602 4	hw mz	cemented sand	46	11	9	2					29	0	sq
42901 A	hw mz	cemented sand	51	16	5	0					15	0	sq
22202 13	hw pl	brown clay	25	10	1	55	10	10	32	2	1	2	rj
40402 2	hw pl	weakly cemented sand	41	10	14	0					34	0	sq
40602 12	hw pl	weakly cemented sand	64	9	11	13					0	1	sq
90402 4	hw pl	weakly cemented sand	42	23	19	5					10	0	sq

Table DR5. Major Element Data for Components of the San Ysidro Fault

Abbreviations: fw = footwall, hw = haning wall, pl = protolith, dz = damage zone, mz = mixed zone.

Sample Number	Fault Zone Component	Lithology	Major Element (All Concentrations in Percent) Si	Al	Fe	Ca	Na	K	Mg	Ti
22202 5	clastic dike	uncemented clastic dike	28	3.35	0.90	0.43	0.98	2.06	0.25	0.16
42901 C	clastic dike	veakly cemented clastic dik	13	2.55	2.06	0.83	0.78	1.94	0.86	0.28
22002 9A	core	green clay	14	5.44	4.49	0.91	0.35	2.83	2.03	0.46
22002 9C	core	tan clay	18	6.56	4.30	0.78	0.46	2.83	1.98	0.45
22202 6	core	green clay	24	8.00	4.45	0.79	0.38	2.74	1.95	0.46
22202 7	core	red clay	26	8.58	4.11	0.77	0.46	2.66	1.89	0.47
40402 3	core	cemented sandy clay	31	5.11	1.66	0.62	0.40	2.18	1.34	0.29
40602 1	core	red clayey sand	27	5.56	2.62	3.71	0.44	1.70	0.97	0.33
40602 10	core	red clay	23	7.32	4.98	0.75	0.43	3.10	1.55	0.46
42601 A	core	green sandy clay	25	4.43	1.55	0.79	0.99	2.24	0.76	0.29
42601 B	core	red sandy clay	25	4.25	1.63	0.72	0.41	1.75	1.89	0.25
42701 B	core	tan clayey sand	25	5.03	2.34	0.78	0.90	2.15	0.98	0.34
42701 C	core	green sandy clay	24	4.22	1.81	0.80	1.07	2.14	0.72	0.32
42801 A	core	red clay	16	6.02	4.32	7.56	0.10	2.10	1.41	0.38
42801 B	core	green clay	22	6.63	4.60	1.15	0.26	2.36	1.54	0.44
42801 C	core	red green clay	19	6.31	5.04	2.47	0.27	2.88	1.51	0.42
42901 B	core	tan sandy clay	22	6.48	3.21	1.19	0.50	2.12	1.20	0.42
90402 2B	core	tan sandy clay	30	5.27	2.31	0.68	0.76	2.02	0.66	0.27
22202 1	fw mz	weakly cemented sand	24	3.20	0.70	0.60	1.08	2.18	0.35	0.10
40602 11	fw mz	weakly cemented sand	33	3.02	0.45	1.38	0.56	1.54	0.31	0.13
42901 D	fw mz	cemented sand	8.2	1.02	0.41	18.80	0.74	1.25	0.14	0.08
42501 T1H	fw mz core contact	cemented sand	11	1.94	0.33	25.70	0.61	0.90	0.14	0.05
42701 A	fw mz core contact	cemented sand	18	2.46	0.42	15.00	0.91	1.39	0.18	0.07
22002 13A	fw pl	cemented sand	15	1.90	0.57	17.00	0.75	1.31	0.17	0.07
22002 13B	fw pl	weakly cemented sand	23	3.02	0.84	0.57	1.15	2.16	0.34	0.13
40402 1	fw pl	cemented sand	25	2.74	0.78	13.90	0.83	1.34	0.19	0.11
40502 1	fw pl	weakly cemented sand	33	4.01	0.74	0.62	1.14	2.12	0.22	0.11
40602 8	fw pl	red clay	23	7.29	3.54	3.27	1.15	2.15	1.36	0.47
40602 9	fw pl	weakly cemented sand	22	6.75	3.32	4.36	0.31	2.28	1.26	0.33
42501 T1PL	fw pl	weakly cemented sand	26	3.80	1.15	0.84	1.21	2.03	0.39	0.18
90402 1	fw pl	cemented sand	23	2.89	1.03	12.60	0.90	1.42	0.19	0.17
22202 12	hw dz	weakly cemented sand	37	4.17	0.79	0.77	1.11	2.05	0.21	0.14
22002 7	hw mz	cemented sand	12	1.67	0.31	23.60	0.66	1.08	0.12	0.05
40602 4	hw mz	cemented sand	27	2.57	0.41	8.86	0.71	1.62	0.15	0.06
42901 A	hw mz	cemented sand	20	2.54	0.61	12.90	0.97	1.49	0.15	0.11
22202 13	hw pl	brown clay	29	8.30	2.75	1.02	0.26	2.01	0.90	0.52
40402 2	hw pl	weakly cemented sand	34	3.89	1.96	1.16	1.14	1.90	0.27	0.26
40602 12	hw pl	weakly cemented sand	31	4.02	1.11	0.50	0.93	1.94	0.36	0.21
40602 6	hw pl	cemented sand	21	1.84	0.30	16.40	0.60	1.09	0.12	0.05
40602 7	hw pl	weakly cemented sand	34	3.14	0.44	0.41	0.88	1.76	0.18	0.08
90402 4	hw pl	weakly cemented sand	30	3.70	1.27	2.78	1.01	1.90	0.26	0.18

Table DR6. Raw Rare Earth Element Data for Components of the San Ysidro Fault

Abbreviations: pl = protolith, dz = damage zone, mz = mixed zone, fw = footwall, hw = hanging wall.

Sample Number	Fault Zone Component	Lithology	Rare Earth Element (All Concentrations in Parts Per Million)												
			La	Ce	Pr	Nd	Sm	Eu	Gd	Tb	Dy	Ho	Er	Tm	Yb
22202 5	clastic dike	uncemented calstic dike	17.7	38.2	3.57	13.7	2.37	0.614	2.16	0.315	2.16	0.394	1.24	0.195	1.37
42901 C	clastic dike	weakly cemented clastic dike	13.8	27.7	3.00	11.9	2.12	0.494	2.02	0.277	1.84	0.314	1.00	0.152	1.02
22002 9A	core	green clay	40.7	72.2	9.22	37.0	6.52	1.300	6.26	0.882	5.70	0.984	2.95	0.430	2.74
22002 9C	core	tan clay	45.0	90.0	10.30	41.7	7.64	1.500	7.53	1.030	6.76	1.140	3.37	0.500	3.14
22202 6	core	green clay	43.0	76.1	9.82	38.4	6.73	1.290	5.56	0.762	5.12	0.859	2.53	0.373	2.33
22202 7	core	red clay	46.7	81.8	10.80	42.6	7.48	1.500	6.32	0.871	5.72	0.969	2.80	0.412	2.58
40402 3	core	cemented sandy clay	22.3	42.6	5.18	20.4	3.56	0.755	2.99	0.420	2.82	0.483	1.48	0.232	1.62
40602 1	core	red clayey sand	34.0	63.2	7.79	31.2	5.52	1.200	5.34	0.772	5.22	0.904	2.85	0.436	2.77
40602 10	core	red clay	52.2	98.8	12.00	47.0	8.39	1.720	7.21	0.965	6.36	1.060	3.10	0.455	2.82
42601 A	core	green sandy clay	21.6	39.8	4.75	18.9	3.32	0.734	3.07	0.432	2.97	0.521	1.69	0.272	1.91
42601 B	core	red sandy clay	22.2	43.2	4.73	18.6	3.33	0.694	3.02	0.432	2.86	0.496	1.53	0.239	1.58
42701 B	core	tan clayey sand	23.5	44.2	5.27	20.6	3.86	0.816	3.35	0.551	3.47	0.642	2.00	0.367	2.26
42701 C	core	green sandy clay	21.9	40.1	4.89	19.6	3.45	0.809	3.35	0.488	3.32	0.586	1.90	0.309	2.12
42801 A	core	red clay	46.6	75.4	9.75	39.0	6.98	1.370	6.79	0.966	6.37	1.110	3.42	0.511	3.39
42801 B	core	green clay	36.9	71.1	8.31	33.1	5.80	1.210	5.75	0.783	5.08	0.874	2.66	0.403	2.50
42801 C	core	red green clay	47.6	104.0	10.50	42.7	7.37	1.420	6.89	0.952	6.15	1.050	3.12	0.460	2.79
42901 B	core	tan sandy clay	36.4	71.2	8.06	32.2	5.76	1.180	5.53	0.762	4.97	0.838	2.56	0.391	2.62
90402 2B	core	tan sandy clay	27.2	55.5	5.96	23.0	4.05	0.889	3.48	0.476	3.19	0.532	1.66	0.261	1.74
22202 1	fw mz	cemented sand	16.8	27.2	3.62	14.4	2.54	0.769	2.50	0.354	2.34	0.405	1.24	0.191	1.19
40602 11	fw mz	cemented sand	16.3	32.9	3.53	13.5	2.33	0.475	1.92	0.256	1.72	0.308	0.96	0.161	1.07
42901 D	fw mz	cemented sand	7.7	8.9	1.60	6.6	1.22	0.321	1.53	0.235	1.82	0.349	1.12	0.174	1.13
30603 2	fw mz	calcite vein	3.8	1.3	0.78	3.6	0.72	0.190	0.95	0.160	1.34	0.316	1.22	0.206	1.57
30603 2	fw mz	calcite cement	10.4	16.3	2.20	8.5	1.46	0.421	1.45	0.208	1.42	0.278	0.99	0.159	1.07
42701 A	fw mz core contact	cemented sand	13.9	15.4	2.60	10.2	1.75	0.504	1.90	0.276	1.93	0.348	1.12	0.166	1.12
42501 T1H	fw mz core contact	cemented sand	8.4	11.5	1.60	6.4	1.19	0.364	1.22	0.181	1.34	0.280	0.96	0.148	0.96
22002 13A	fw pl	cemented sand	13.3	16.0	2.60	10.3	1.80	0.502	1.91	0.273	1.87	0.334	1.10	0.166	1.04
22002 13B	fw pl	weakly cemented sand	18.5	29.8	3.94	15.6	2.69	0.792	2.66	0.377	2.42	0.420	1.32	0.197	1.35
40402 1	fw pl	cemented sand	18.7	21.3	3.72	15.3	2.80	0.695	2.97	0.438	3.20	0.597	1.92	0.301	1.84
40502 1	fw pl	weakly cemented sand	17.1	27.9	3.54	13.6	2.40	0.657	2.07	0.289	1.94	0.334	1.04	0.160	1.04
40602 8	fw pl	red clay	36.3	74.3	8.40	33.2	5.94	1.250	5.51	0.780	5.15	0.873	2.65	0.397	2.59
40602 9	fw pl	weakly cemented sand	32.6	61.7	7.30	29.0	5.28	1.080	4.83	0.688	4.60	0.806	2.49	0.384	2.48
42501 T1PL	fw pl	weakly cemented sand	17.3	35.9	3.86	15.2	2.70	0.754	2.54	0.368	2.41	0.427	1.34	0.201	1.31
90402 1	fw pl	cemented sand	17.6	25.4	3.62	14.1	2.42	0.578	2.33	0.335	2.37	0.458	1.52	0.237	1.55
22202 12	hw dz	weakly cemented sand	19.4	34.4	4.04	15.2	2.47	0.657	2.07	0.296	1.95	0.347	1.08	0.168	1.15
22002 7	hw mz	cemented sand	8.8	10.5	1.80	7.5	1.39	0.436	1.66	0.248	1.97	0.394	1.34	0.204	1.34
40602 4	hw mz	cemented sand	19.7	23.3	3.50	13.4	2.18	0.586	2.00	0.279	2.04	0.386	1.28	0.200	1.32
42901 A	hw mz	cemented sand	15.6	24.9	3.17	12.3	2.10	0.533	1.91	0.272	1.80	0.313	0.99	0.153	1.04
22202 13	hw pl	brown clay	41.3	68.6	9.03	34.7	6.10	1.210	5.20	0.727	4.83	0.825	2.55	0.388	2.46
40402 2	hw pl	weakly cemented sand	27.0	51.5	5.66	21.4	3.47	0.781	2.90	0.397	2.69	0.483	1.56	0.246	1.68
40602 12	hw pl	weakly cemented sand	18.0	31.6	3.76	14.2	2.36	0.622	2.04	0.273	1.93	0.330	1.09	0.176	1.15
40602 6	hw pl	cemented sand	18.9	14.7	3.28	12.5	2.19	0.583	2.41	0.367	2.73	0.516	1.67	0.270	1.83
40602 7	hw pl	weakly cemented sand	15.6	24.8	3.32	12.5	2.13	0.569	1.89	0.263	1.81	0.310	0.99	0.147	0.95
90402 4	hw pl	weakly cemented sand	20.8	35.5	4.48	17.2	2.86	0.708	2.50	0.344	2.23	0.386	1.19	0.188	1.28

Table DR7. Permeametry Data from Fault Components of the San Ysirdo Fault

All values from liquid permeametry except fault core clays from mercury injection capillary pressure permeametry. Directions of permeability are relative to the nominal plane of the fault zone. Abbreviations: FW = footwall, HW = hanging wall, max = maximum, min = minimum, micep = Mercury Injection Capillary Entry Pressure, perm = permeability, geomean = geometric mean, n = number of samples, k = permeability, m = meters.

Sample Number	Core Direction Relartive to Bedding	Fault Zone Component	Structural Location	Lithology	k (m^2)	Magnitude of Anisotropy	kmax Direction	Measurement Technique
42601 B	unoriented	core		red sandy clay	3.0E-20			micep
42701 E	unoriented	core		red clay	5.5E-20			micep
42801 B	unoriented	core		green clay	7.7E-20			micep
42601 C	unoriented	core		brown sandy clay	1.8E-19			micep
42901 B	unoriented	core		tan sandy clay	2.7E-19			micep
42801 A	unoriented	core		red clay	4.4E-19			micep
42801 C	unoriented	core		red green clay	7.5E-19			micep
42601 A	unoriented	core		green sandy clay	1.8E-15			micep
22002 9A	unoriented	core		green clay	1.4E-19			micep
40602 1	unoriented	core		red clayey sand	2.9E-18			micep
40602 10	unoriented	core		red clay	3.2E-20			micep
90602 7A	unoriented	core		red clay	9.6E-20			micep
90602 7B	unoriented	core		red clay	5.2E-20			micep
42501 T1HA	parallel	mixed zone	footwall	cemented sand	4.3E-18			liquid perm
42501 T1HA	perpendicular	mixed zone	footwall	cemented sand	5.9E-18	1.37	perpendicular	liquid perm
42701 A	parallel	mixed zone	footwall	cemented sand	1.1E-16			liquid perm
42701 A	perpendicular	mixed zone	footwall	cemented sand	5.6E-17	2.00	parallel	liquid perm
40402 4	parallel	mixed zone	footwall	cemented sand	2.7E-17			liquid perm
40402 4	perpendicular	mixed zone	footwall	cemented sand	5.1E-17	1.87	perpendicular	liquid perm
42501 TB 1	parallel	mixed zone	footwall	cemented sand	2.7E-15			liquid perm
42501 TB 1	perpendicular	mixed zone	footwall	cemented sand	2.5E-16	10.7	parallel	liquid perm
22002 10	parallel	mixed zone	footwall	cemented sand	3.2E-18			liquid perm
22002 10	perpendicular	mixed zone	footwall	cemented sand	3.0E-18	1.05	perpendicular	liquid perm
22002 11	parallel	mixed zone	footwall	cemented sand	4.1E-17			liquid perm
40602 11	parallel	mixed zone	footwall	cemented sand	1.0E-17			liquid perm
42501 T1 PL	parallel	protolith	hanging wall	weakly cemented sand	7.5E-13			liquid perm
40602 7	parallel	protolith	hanging wall	weakly cemented sand	8.4E-13			liquid perm
90402 4	parallel	protolith	hanging wall	weakly cemented sand	1.6E-12			liquid perm
90402 1	parallel	protolith	footwall	cemented sand	6.0E-18			liquid perm
22002 13A	parallel	protolith	footwall	cemented sand	4.0E-17			liquid perm
22002 13B	parallel	protolith	footwall	weakly cemented sand	3.4E-13			liquid perm
40402 1	parallel	protolith	footwall	cemented sand	1.0E-16			liquid perm
40402 2	parallel	protolith	hanging wall	weakly cemented sand	4.1E-12			liquid perm
40502 1	parallel	protolith	footwall	weakly cemented sand	6.8E-12			liquid perm
40602 6	parallel	protolith	hanging wall	cemented sand	8.4E-17			liquid perm
40602 12	parallel	protolith	hanging wall	weakly cemented sand	9.0E-15			liquid perm